No. 94-S1-O-16

FOURTEENTH INTERNATIONAL TECHNICAL CONFERENCE ON THE ENHANCED SAFETY OF VEHICLES

May 23-26, 1994
Munich, Germany

FINITE ELEMENT MODELING AND ANALYSIS OF THORAX/RESTRAINT SYSTEM INTERACTION

Gordon R. Plank
Volpe National Transportation Systems Center
Research and Special Programs Administration
United States Department of Transportation
Kendall Square
Cambridge, Massachusetts 02142
Tel: (617)494-2390

Michael Kleinberger, Rolf H. Eppinger
Office of Crashworthiness Research
National Highway Traffic Safety Administration
United States Department of Transportation
400 Seventh Street, S.W.
Washington, DC 20590

Finite Element Modeling and Analysis of Thorax/Restraint System Interaction

Gordon R. Plank
Volpe National Transportation Systems Center
Research and Special Programs Administration
United States Department of Transportation
Paper No. 94-S1-O-16

Michael Kleinberger, Rolf H. Eppinger
Office of Crashworthiness Research
National Highway Traffic Safety Administration
United States Department of Transportation

ABSTRACT

Various modeling techniques are playing an increasingly important role as a cost effective means of supplementing crashworthiness data for gaining a better understanding of the injury mechanisms associated with automotive crashes. The interaction of a geometrically accurate (50th percentile male) finite element model of the human thorax, and finite element models of a seat belt restraint system and an airbag are examined. Optimization of the thorax model under frontal impact conditions as well as the development of an improved shoulder structure are discussed. Using LSDYNA3D, the three-dimensional finite element structural analysis code, stress fields within the thorax model are examined and the results, using each restraint system in a comparable impact environment, are presented.

INTRODUCTION

A geometrically accurate, finite element model of the human thorax has been developed and exercised using LSDYNA3D, a finite element solver from Livermore Software Technology Corporation (LSTC). Figure 1 illustrates the baseline mesh for this model. The model is represented by a segmented spinal column consisting of twelve thoracic and five lumbar vertebrae and the associated intervertebral disks, twelve ribs, back, abdominal and intercostal muscles, homogeneous viscera and concentrated masses representing the head, arms and lower torso. Also shown in the figure is a rigid body impactor that was used to determine force/deflection characteristics of the model. The model has been validated and optimized by subjecting it to impact conditions specified in Title 49, Part 572 of the Code of Federal Regulations (CFR) which prescribes an impactor weight of 51.5 pounds, with an initial velocity of 22 feet/second. The results of this impact are compared to force/deflection data that has been gathered on cadavers[1-3] and scaled to a 50th percentile male[4].

MESH DEVELOPMENT

In earlier work[5], mesh generation was accomplished with INGRID, the mesh generating software that accompanies DYNA3D[6], the dynamic solver provided by Lawrence Livermore Laboratories (LLL). Early development of the mesh for the geometrically accurate thorax[7] was accomplished primarily with DISPLAY, mesh generating software from the Engineering Mechanics Research Corporation. Current mesh generation and model manipulation are being performed with PATRAN from PDA Engineering. The dynamic solver used in earlier work was DYNA3D from LLL while LSDYNA3D from LSTC is being used for the current work. The geometry used in the current model was based primarily on data published by Roberts and Chen[8], other available anthropometry[9,10] and cross-sectional anatomy[11]. The model was then scaled to represent a 50th percentile male. All elements in the thorax model are eight-node solids.

MATERIAL PROPERTIES

An accurate representation of the properties of biological materials presents the biggest challenge to the modeler of human body parts. There is ample information on the properties of stiff materials like bone that are relatively easy to characterize in the laboratory. On the other hand, for soft biological materials, there is little or, in many cases, no information available that is directly applicable for use in

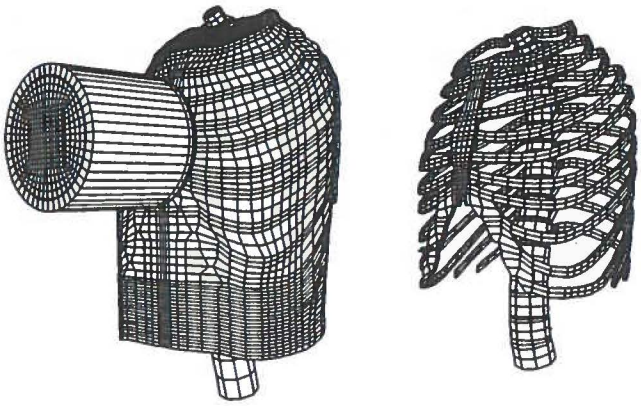

a. Thorax Model with Impactor b. Skeletal Portion

Figure 1. Baseline Thorax Model

finite element analysis. For the models developed in the current work, material properties have been taken from the literature[12-17]. The bone, cartilage, and ligaments have been represented by linear elastic materials while the interior thoracic volume and some of the muscle elements have been represented by a viscoelastic property defined by the following equation for the shear modulus G.

$$G(t) = G_L + (G_S - G_L)\varepsilon^{-\beta t}$$

where:

G_S = short term shear modulus
G_L = long term shear modulus
β = decay constant

RESULTS AND DISCUSSION

BASELINE MODEL

Figure 2 is an illustration of the baseline model subjected to impact conditions specified in Part 572 of the CFR. It can be seen at t = 0.02 sec. in Figure 2 that there is significant extrusion of the softer interior material at the top and excessive spreading of the ribs, both of which contribute to excessive compliance of the model. Figure 3 illustrates the force/deflection characteristics of this impact. In addition to the model response, Figure 3 shows the recommended response corridor based upon data gathered in the field on cadavers[1-4]. The results confirm that this model was too compliant, that is, there was too much deflection along the impactor center line and force levels did not attain values that were acceptable. This was somewhat anticipated as the material properties used were obtained from an earlier 7-rib model[5] with a geometry that was considerably stiffer to frontal impact than the present configuration.

BASELINE MODEL OPTIMIZATION

Several things were done to optimize the response of the current model including capping the top with a layer of relatively stiff elements, stiffening the intercostal muscle elements, adjusting the shear modulus G of the interior

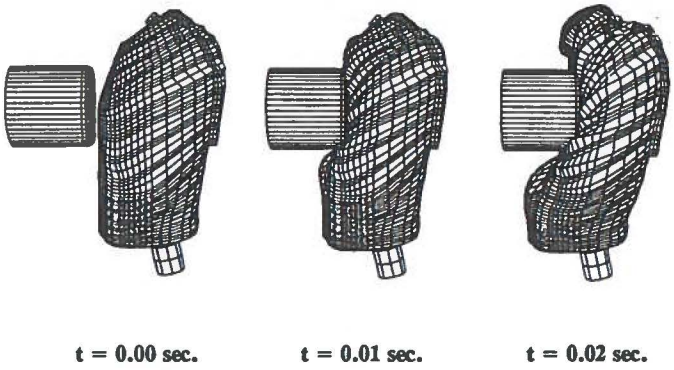

t = 0.00 sec. t = 0.01 sec. t = 0.02 sec.

Figure 2. Baseline Model Under Part 572 Impact Side View

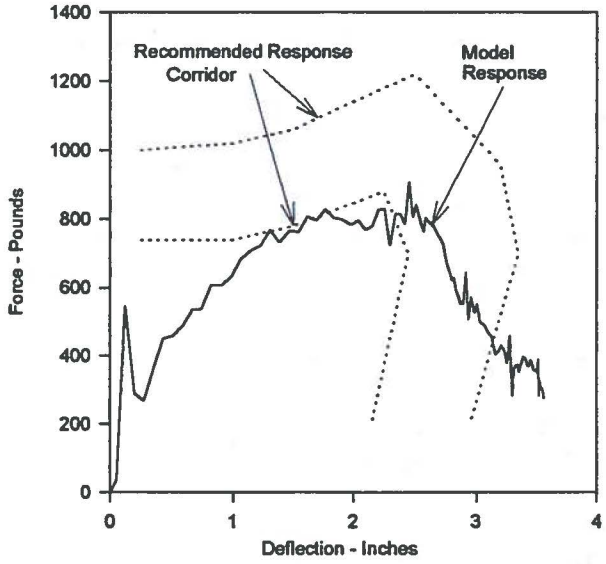

Figure 3. Force/Deflection Characteristics (Baseline Model - Impactor Initial Velocity = 22 feet/sec.)

material and modifying the sternal mass.

Capping Interior Material

As seen in Figure 2, under impact, the interior material is extruded up through the top in a way that is not observed in actual testing due to the presence of additional structure (clavicle, head and neck). To eliminate this problem, the top layer of elements was given an elastic modulus of E = 1.5×10^3. The effect on the response is shown in Figure 4. It can be seen that the interior material no longer extrudes from the top but the spreading of the ribs has become more exaggerated, especially between the upper ribs. The force/deflection characteristics are shown in Figure 5. Although the interior material no longer extrudes from the top, it can be seen that the response characteristics did not change significantly.

Intercostal Muscle Modification

It can also be seen in Figure 2 that in addition to excessive spreading of the ribs in the model, the intercostal muscles bulge unrealistically. The material properties used

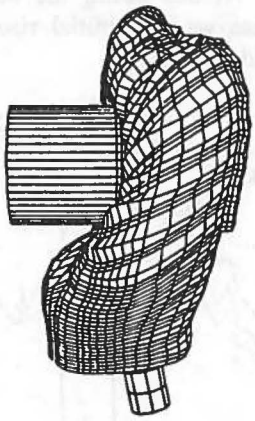

t = 0.02 sec.

Figure 4. Baseline Model Under Part 572 Impact Capped Interior Material (Side View) (Impactor Initial Velocity = 22 feet/sec.)

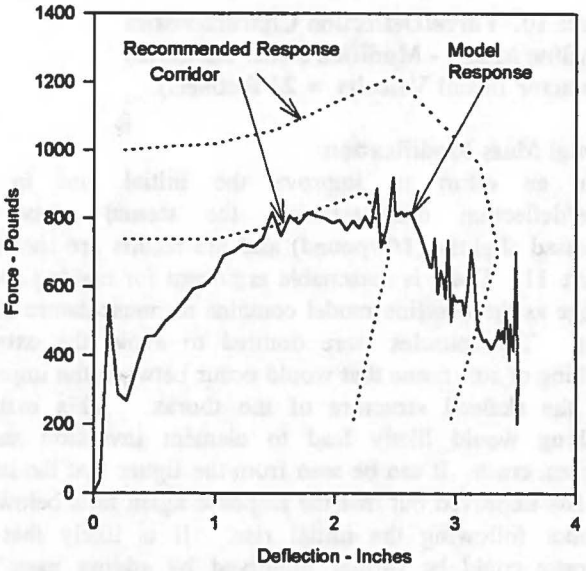

Figure 5. Force/Deflection Characteristics (Baseline Model - Capped Interior Material) (Impactor Initial Velocity = 22 feet/sec.)

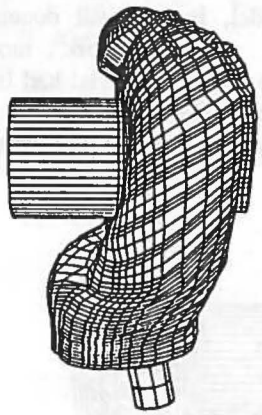

t = 0.02 sec.

Figure 6. Baseline Model Under Part 572 Impact Modified Intercostal Muscles (Side View) (Impactor Initial Velocity = 22 feet/sec.)

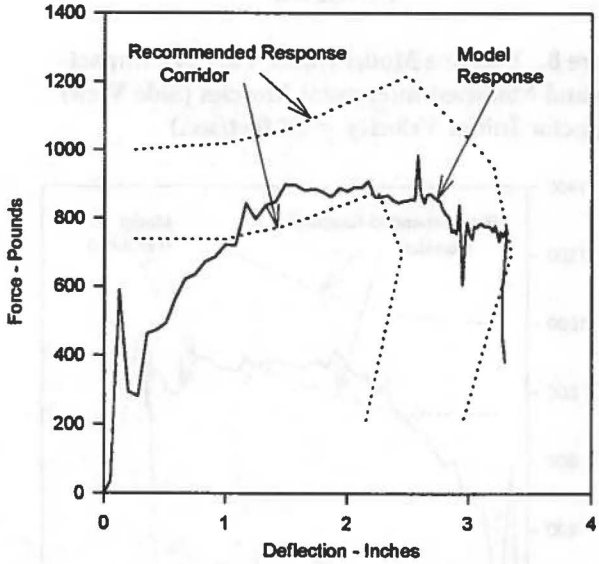

Figure 7. Force/Deflection Characteristics (Baseline Model - Modified Intercostal Muscles) (Impactor Initial Velocity = 22 feet/sec.)

for the intercostal muscles were based on laboratory data from samples of isolated muscle tissue. Intercostal tissue actually contains numerous other materials (nerves, fascia, blood vessels) that tend to give it a much stiffer characteristic. The intercostal muscles were given an elastic modulus of $E = 1.5x10^3$ and the resulting response is shown in Figure 6. It is apparent from the figure that the ribs no longer spread and the intercostal muscles no longer bulge as they did previously but the interior material now extrudes even more dramatically from the top. Figure 7 illustrates that this modification had a greater effect on the force/deflection characteristics than capping the interior material.

The impact response of the model when applying both of the above modifications (cap and stiffened intercostal muscles) is shown in Figure 8. There is no longer spreading of the ribs or extrusion of softer interior material and the abdomen is seen to protrude in a manner similar to what is seen in actual tests. The resulting force/deflection characteristics can be seen in Figure 9 where further improvement is noted. The maximum deflection observed is now within the recommended corridor. An adequate force level has still not been achieved however, and additional modifications were required.

Shear Modulus Modification

A parameter that was of great importance in the current model was the shear modulus G of the interior material. There is very little data in the literature for this parameter. In many cases however, the long term shear modulus G_L can be inferred from static measures of elastic modulus which are more commonly reported. The short term shear modulus G_S,

which, as will be seen, has a large effect on the dynamic response of the model, is not well documented for most biological materials. In earlier work[5], modification of the shear modulus of the interior material had little effect on the force/deflection characteristics of the model. In that model, which was not an anthropometrically accurate representation,

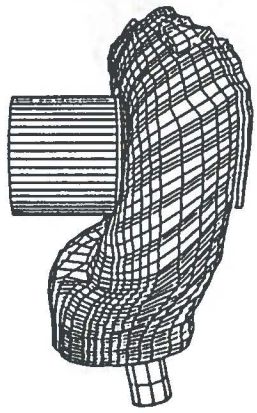

t = 0.02 sec.

Figure 8. Baseline Model Under Part 572 Impact Cap and Modified Intercostal Muscles (Side View) (Impactor Initial Velocity = 22 feet/sec.)

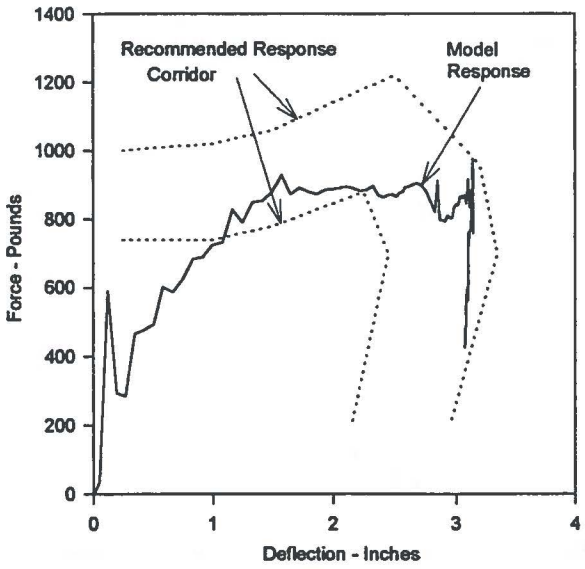

Figure 9. Force/Deflection Characteristics (Baseline Model - Cap and Modified Intercostal Muscles) (Impactor Initial Velocity = 22 feet/sec.)

the impact response was dominated by the rib geometry. While yielding an acceptable global force/deflection characteristic, individual ribs did not exhibit appropriate bending characteristics. The current model exhibits much more sensitivity to changes in shear modulus. The short term shear modulus was increased and applied in combination with the two modifications discussed above. The results are shown in Figure 10.

As seen in the figure, a short term shear modulus of G_S = 8.57 psi results in most of the impact response falling within the recommended corridor. This value of G_S was used in all subsequent testing. At this point, the only unsatisfactory aspect of the response was the initial rise, which was not within the recommended corridor.

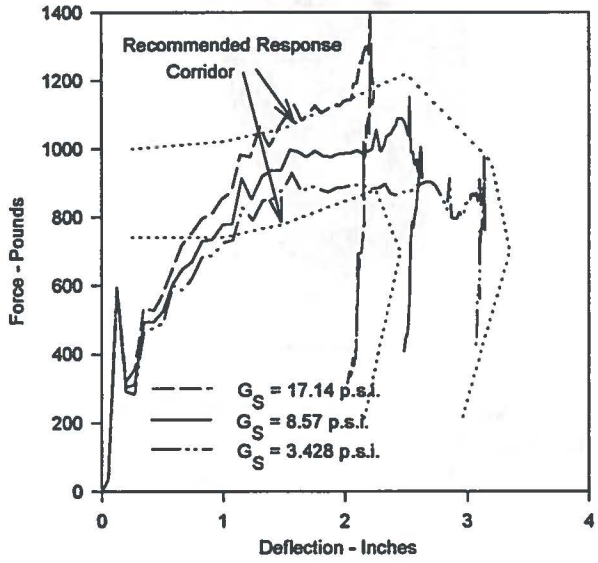

Figure 10. Force/Deflection Characteristics (Baseline Model - Modified Shear Modulus) (Impactor Initial Velocity = 22 feet/sec.)

Sternal Mass Modification

In an effort to improve the initial rise in the force/deflection characteristics, the sternal mass was increased slightly (1/2 pound) and the results are shown in Figure 11. There is reasonable argument for making such a change as the baseline model contains no musculature at the front. The muscles were omitted to avoid the extreme crushing of soft tissue that would occur between the impactor and the skeletal structure of the thorax. This extreme crushing would likely lead to element inversion and a program crash. It can be seen from the figure that the initial rise has improved but that the response again falls below the corridor following the initial rise. It is likely that the response could be further improved by adding mass just behind the sternum in such a way that the impactor encounters the additional mass in an incremental fashion. Without a well founded physical argument for making such a change, this issue was not pursued further. It was also felt that development of discrete organs in the future may have a significant effect on the initial rise of the force/deflection response of the model. The current configuration then, was considered to be a reasonable representation and as good as could be achieved at this time. The material characteristics that were used in this model are summarized in Table 1. This configuration was used in the development of contact surface models.

CONTACT SURFACE DEVELOPMENT

The thorax model has been tested with two contact surface models; a diagonal driver side seat belt and an airbag. The input pulse to both models was a ramp velocity of 0 to 264 inches per second (15 mph) from 0 to 100 milliseconds and then maintained at 264 inches per second for another 100 milliseconds.

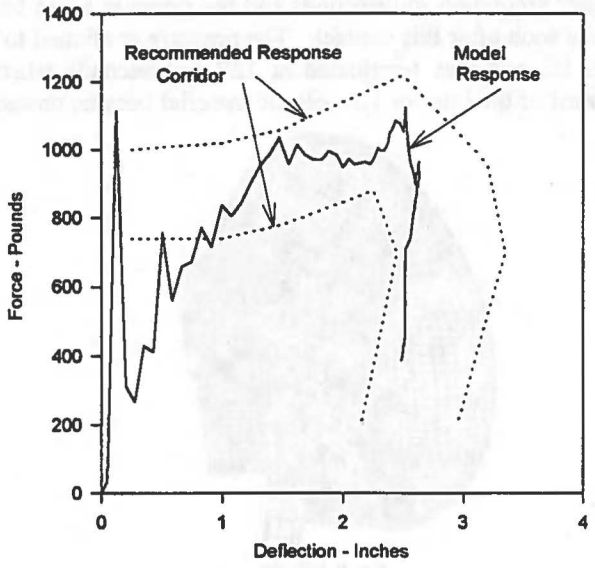

Figure 11. Force/Deflection Characteristics Sternal Mass Modification (Impactor Initial Velocity = 22 feet/sec.)

Table 1
Model Material Properties for the Thorax Model
(Units are in pounds, inches and seconds)

Bone	**Intervertebral Disks**
$E = 1.75 \times 10^6$ Poisson's Ratio = .3 Density = 1.73×10^{-4}	$E = 1.5 \times 10^3$ Poisson's Ratio = .2 Density = 1.0×10^{-4}
Viscoelastic Interior	**Intercostal Muscles**
$K = 41.7$ $G_S = 8.570$ $G_L = .3428$ Density = 1.0×10^{-4} $\beta = 100$	$E = 1.5 \times 10^3$ Poisson's Ratio = .3 Density = 1.0×10^{-4}
Cartilaginous Elements	**Abdominal Muscles**
$E = 3.00 \times 10^{-3}$ Poisson's Ratio = .46 Density = 1×10^{-4}	$K = 66.6$ $G_S = 10.170$ $G_L = 3.390$ Density = 1.0×10^{-4} $\beta = 100$
Ligamentous Elements	**Back Muscles**
$E = 1.74 \times 10^{-3}$ Poisson's Ratio = .42 Density = 1.0×10^{-4}	$K = 33.3$ $G_S = 10.350$ $G_L = 3.448$ Density = 1.0×10^{-4} $\beta = 100$

Seat Belt Model

The seat belt model (Figure 12) consisted of triangular shell elements. The belt was two inches wide and was represented as a linear elastic material with $E = 5.0 \times 10^4$ psi., resulting in a elongation of 20 percent under a tension of 2,500 pounds. The ramp input velocity described above was applied in a rearward direction at each end of the belt and the thorax itself was free to move in any direction. The contact interface had a coefficient of friction of .5. In an earlier implementation of the seatbelt, four-node shell

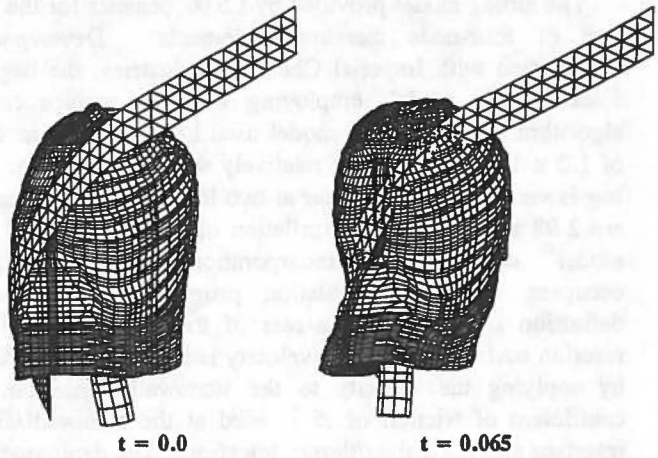

Figure 12. Thorax/Seatbelt Configuration

elements were used and significant hourglassing was experienced with these elements. Hourglassing is not possible with triangular elements and the current seat belt model performed well. In Figure 12, significant deformation of the thorax is noted at t = 0.065 seconds.

Figure 13 illustrates the thorax/seatbelt model under severe impact. Only the skeletal portion of the model is shown as an examination of the stress in the ribs is desired. Of particular interest in this figure is the stress distribution away from the belt. A high stress region is noted in the ribs in the upper right quadrant. The darkest portions of the illustration represent areas where the stress exceeds 7,000 psi. In recent belt tests with cadavers performed for the NHTSA, rib fracture was noted in the upper right quadrant

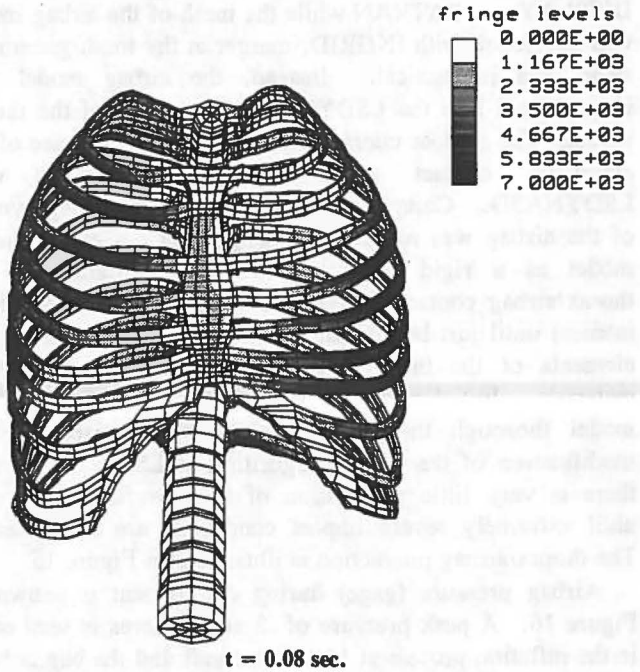

Figure 13. Stress Contours Under Severe Impact (Thorax/Seatbelt Model)

under severe impact conditions. The thorax/seatbelt model in Figure 13 confirms the potential for this fracture.

Airbag Model

The airbag model provided by LSTC consists for the most part of four-node membrane elements. Developed in cooperation with Imperial Chemical Industries, the bag is a folded fabric model, employing a single surface contact algorithm. The material model used has an elastic modulus of 1.2×10^5 psi making it relatively stiff in distension. The bag is vented toward the rear at two locations with holes that are 2.98 in^2 in area. The inflation of the bag is based on a model[18] developed for incorporation into the CAL3D[19] occupant dynamics simulation program. A stonewall definition is placed at the rear of the airbag model as a reaction surface. The ramp velocity is imparted to the airbag by applying the velocity to the stonewall definition. A coefficient of friction of .5 is used at the stonewall/airbag interface and the airbag/thorax interface. The deployment of the airbag is illustrated in Figure 14.

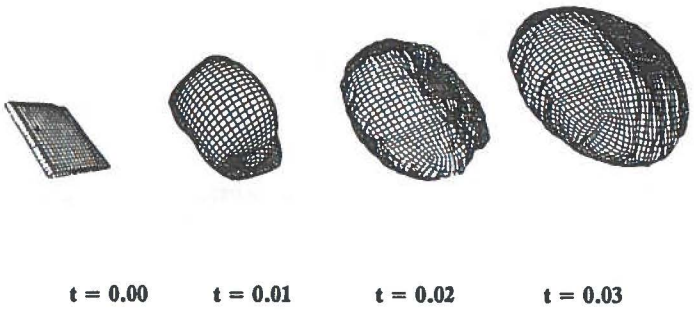

Figure 14. Airbag Model Deployment

Since the mesh of the thorax model was developed with DISPLAY and PATRAN while the mesh of the airbag model was developed with INGRID, merger at the mesh generation stage was impractical. Instead, the airbag model was incorporated into the LSDYNA3D input deck of the thorax model. The contact interface was implemented by use of the automatic contact input generation provided with LSDYNA3D. Computational overhead during deployment of the airbag was reduced by designating the entire thorax model as a rigid body and delaying initiation of the thorax/airbag contact interface calculations (computationally intense) until just before contact is made. At this point, the elements of the thorax are switched back to deformable materials. Initial problems with penetration of the thorax model thorough the shell elements were corrected with modification of the contact algorithm at LSTC. Currently there is very little penetration of the interfaces observed, until extremely severe impact conditions are encountered. The thorax/airbag interaction is illustrated in Figure 15.

Airbag pressure (gage) during deployment is shown in Figure 16. A peak pressure of .8 atmospheres is seen early in the inflation process at 11 milliseconds and the bag is fully inflated at 30 milliseconds. It is then undisturbed and deflating through the vent holes until the thorax makes contact around 66 milliseconds and the pressure again begins to rise soon after this contact. The pressure continued to rise until the test was terminated at 120 milliseconds when an element of the interior viscoelastic material became unstable.

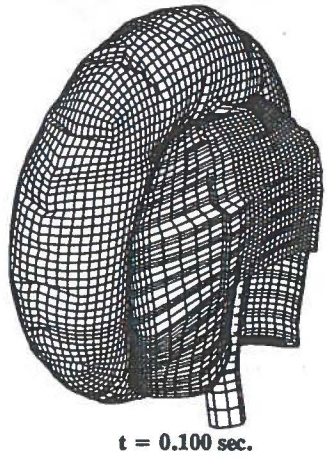

Figure 15. Thorax/Airbag Interaction

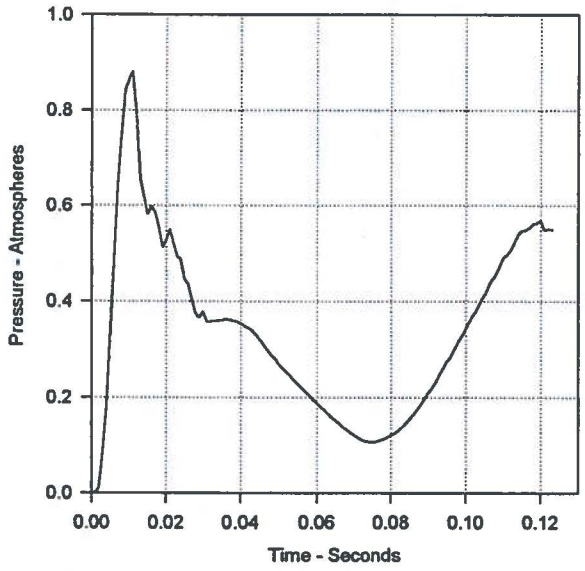

Figure 16. Airbag Pressure (gage) During Deployment

Seatbelt - Airbag Comparison

Early in the contact surface model development, problems were encountered with instability of viscoelastic elements under severe impact. To insure element survival in seatbelt/airbag comparison tests, it was required to increase the bulk modulus of these materials by an order of magnitude. In addition, Poisson's ratio for the intercostal muscles was increased from .3 to .499. With the currently available material models this is often necessary in cases of very large deformation. The thorax model with these changes was used to measure relative performance of the seatbelt and airbag models.

To compare the performance of the seat belt and airbag, thorax deflection, spine velocity and acceleration at the level of the impactor in the Part 572 tests have been observed for both restraint system models. Figure 17 illustrates the mid-line deflection of the thorax model as it encounters each

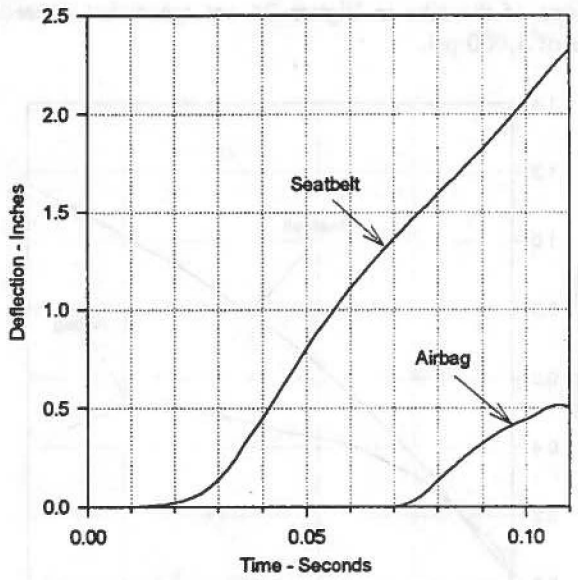

Figure 17. Thorax Deflection

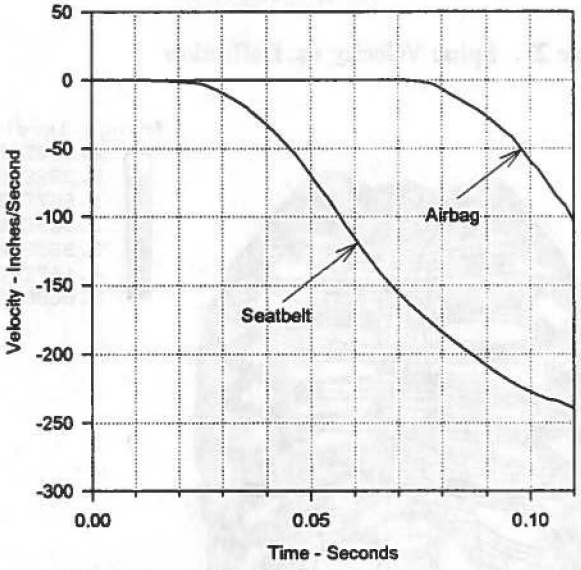

Figure 18. Spine Velocity

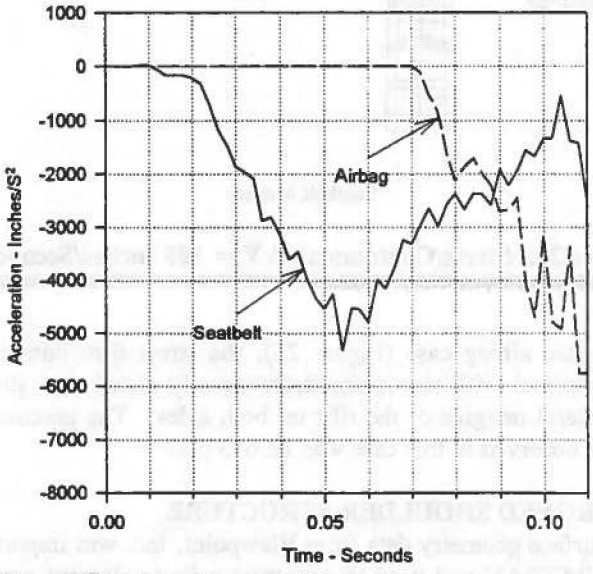

Figure 19. Spine Acceleration

restraint system. Mid-line deflection is defined as the reduction in distance between two nodes in the thorax along the centerline of the impactor. One node is on the posterior surface of the sternum and the other is on the anterior surface of a vertebra. Thorax deflection when contacting the airbag occurs much later than in the seatbelt case and the deflection itself is considerably less. Figure 18 illustrates the spine velocity for each of the restraint system models and Figure 19 illustrates the accelerations experienced with each restraint system at that same point. Velocity and acceleration have been measured at the above mentioned node on the spine.

As can be seen in Figures 17, 18 and 19, the two tests are considerably out of phase, that is, the thorax makes contact with the seat belt almost immediately while, in the airbag case, contact is made after approximately 66 milliseconds. It is helpful to normalize the data by plotting time histories after the initial contact with the restraint system. Initial contact is assumed to have occurred when there is a perceptible deflection of the thorax. This happens at t = .008 seconds with the seatbelt model and at t = .066 seconds with the airbag model. Normalized representations of deflection, velocity and acceleration are shown in Figures 20, 21 and 22.

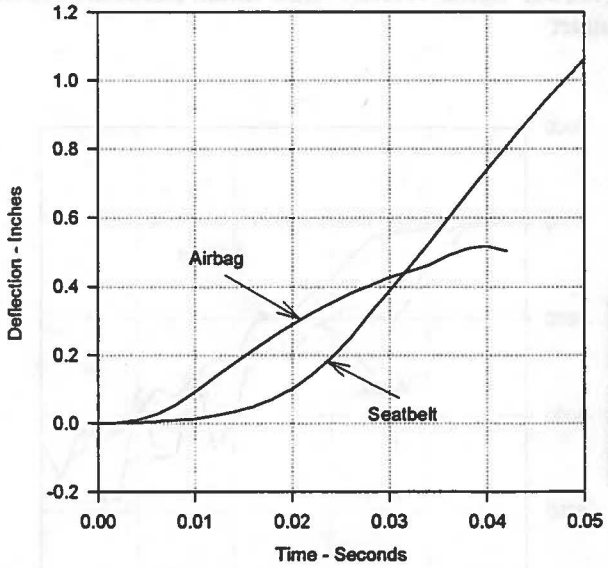

Figure 20. Thorax Deflection After Initial Restraint System Contact

The difference in the dynamic response of the thorax in the two cases shown is significant. Figure 20 indicates that after initial contact the thorax deflection due to the airbag is greater than that due to the seatbelt until about 32 milliseconds when deflection due to the seatbelt becomes greater. Figures 21 and 22 show remarkable similarities between the two cases in the shape of the time histories of velocity and acceleration with a slight phase difference implying a more rapid onset of both parameters for the airbag model.

A better performance comparison can be made by observing the critical parameters as a function of the change in velocity of the thorax. Figure 23 illustrates the mid-line deflection for the two models as a function of velocity. It

can be seen that after a common change in velocity of 105 inches/second (approximately 6 miles/hour), the mid-line deflection for the thorax/seat belt model is approximately 1.04 inches while that for the thorax/airbag model is only .5 inches, a significant difference.

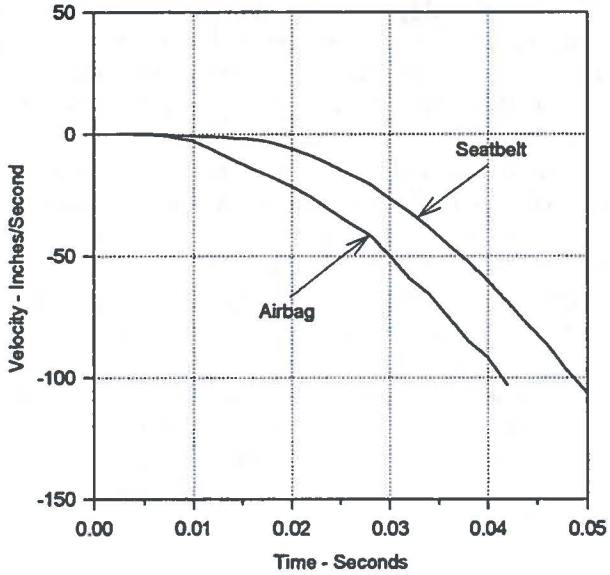

Figure 21. Spine Velocity After Initial Restraint System Contact

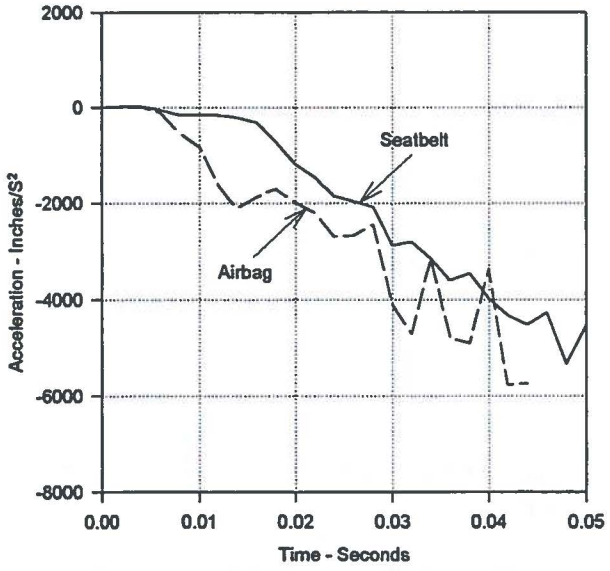

Figure 22. Spine Acceleration After Initial Restraint System Contact

Figure 24 is an illustration of the bony structure of the thorax after a velocity change of 105 inches/second for the seatbelt model and Figure 25 illustrates the airbag model at the same change in velocity. It can be seen that there is a difference in the stress distribution for each case as would be expected.

In the seatbelt case there is significant asymmetry as would be expected. The stress distribution is determined by the course of the belt, and maximum stresses appear to occur where bending moments in the ribs are greatest. In this case the maximum stress observed was 14,970 psi. The darkest portions of the ribs in Figure 24 are areas that exceeded a stress of 5,000 psi.

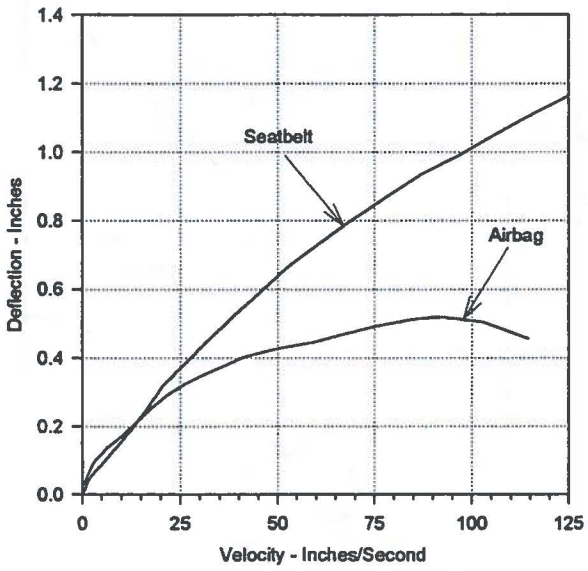

Figure 23. Spine Velocity vs. Deflection

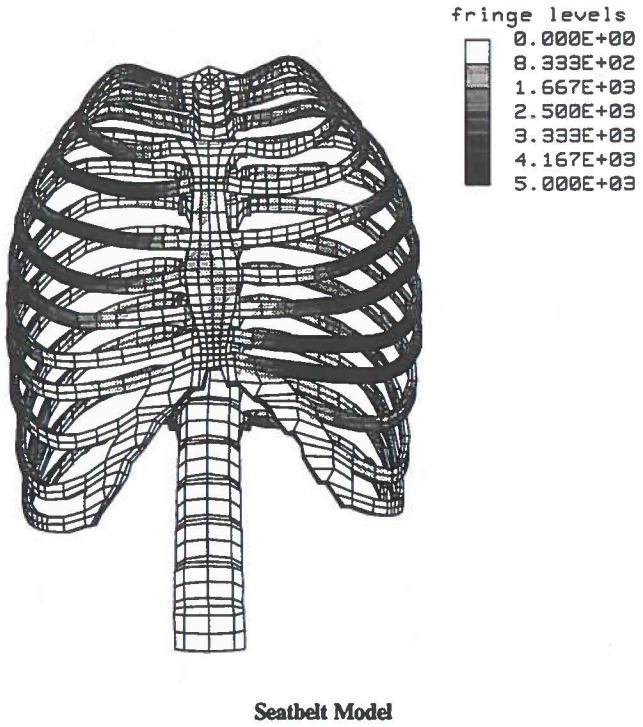

Figure 24. Stress Contours at $\Delta V = 105$ Inches/Second (Maximum Principal Stress)

In the airbag case (Figure 25), the stress distribution is symmetrical with maximum stress equally distributed along the lateral margins of the ribs on both sides. The maximum stress observed in this case was 12,665 psi.

IMPROVED SHOULDER STRUCTURE

Surface geometry data from Viewpoint, Inc. was imported into PATRAN and used to construct a finite element model of the shoulder girdle consisting of a scapula, clavicle and

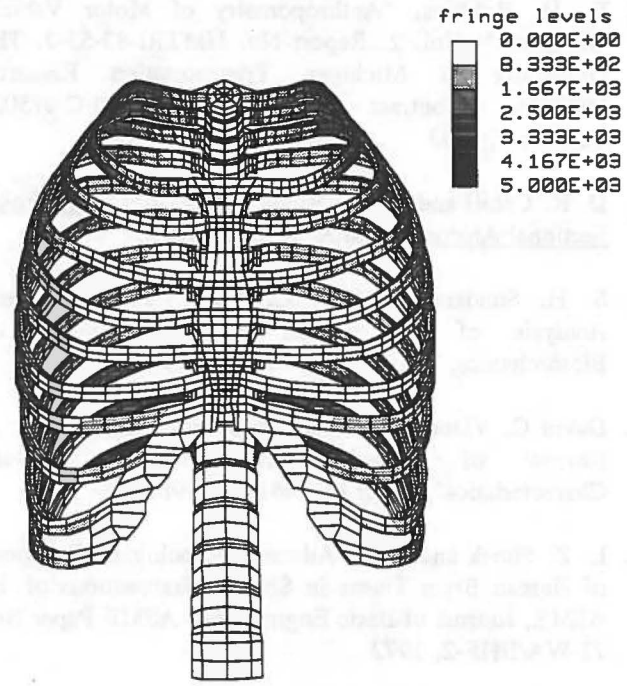

Figure 25. Stress Contours at $\Delta V = 105$ Inches/Second (Maximum Principal Stress)

the ligaments connecting the two (Figure 26). The shape of the structure was adjusted slightly to fit the current thorax model.

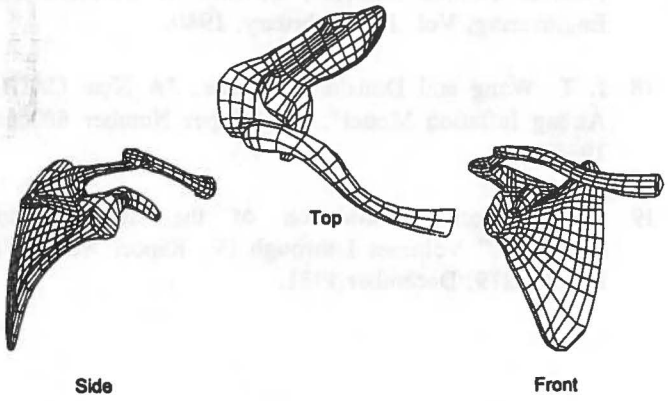

Figure 26. Scapula/Clavicle Structure

Maintaining an accurate shape of the shoulder structure made it difficult to connect the structure to the existing thorax model. Tying the two with muscle elements by equivalencing of nodes was virtually impossible and the surfaces will be connected as tied interfaces in LSDYNA3D.

Figure 27 illustrates the bony portion of the shoulder girdle as it appears incorporated into the thorax model. This model will be tested under PART 572 conditions to determine if the shoulder structure has any effect on the response to frontal impact. It is anticipated that there will be changes in the response using a seatbelt as the belt will pass over the shoulder structure.

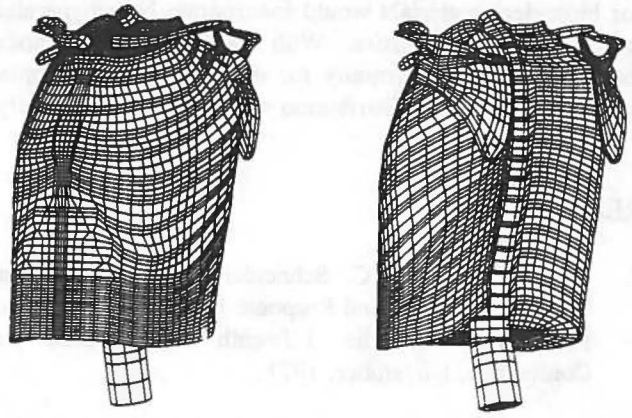

Figure 27. Thorax/Shoulder Complex

FUTURE WORK

Work planned for the future will include additional restraint system analyses with a complete thorax/shoulder girdle complex, the development of rigid body extremities, side impact testing and the development of discrete intrathoracic organs.

CONCLUSIONS

The current geometrically accurate finite element model of the human thorax represents a useful tool for the analysis of frontal impact. The model will be of great use in the optimization of contact surfaces such as seatbelts, airbags, steering wheels and other interior structures. The current thorax/seatbelt model successfully confirmed the potential for rib fracture in the upper right quadrant of the thorax away from the belt line, a phenomenon that had been experienced in the field under similar impact conditions. An improved shoulder structure promises to result in more reliable testing of restraint system models, especially seat belts and will play an important role in side impact tests.

Regarding the comparison of airbag and seatbelt performance, several tentative conclusions may be drawn. Under comparable impact conditions (i.e. after a common change in velocity), mid-line deflection of the thorax is significantly less with an airbag restraint system than with a diagonal seatbelt restraint system. In addition, rib stress is less with the airbag model than with the seatbelt model. Lateral stress symmetry is observed in the airbag case, distributing the load more uniformly.

There remain several issues that are of significant importance. Among these is the lack of information on the material properties of intercostal muscles. Until this information is available, there will remain uncertainty in the combined effect of intercostal muscle stiffness and short term shear modulus on thoracic force/deflection characteristics.

The limited availability of appropriate material models for anatomical simulations in LSDYNA3D or public domain DYNA3D presents another problem. A very useful model

for biological materials would incorporate both hyperelastic and viscoelastic properties. With improved material models, there will be an opportunity for modeling thoracic contents and examining strain distribution within the thoracic cavity.

REFERENCES

1. C. K. Kroell, D. C. Schneider, and A. M. Nahum, "Impact Tolerance and Response of the Human Thorax", Proceedings of the Fifteenth Stapp Car Crash Conference, November, 1971.

2. T. E. Lobdel, C. K. Kroell, D. C. Schneider, W. E. Hering, and A. M. Nahum, "Impact Response of the Human Thorax", Human Impact Response - Measurement and Simulation. Proceedings of Symposium at General Motors Research Laboratories, Oct. 2, 3, 1972, edited by W. F. King and H. J. Mertz, London: Plenum Press.

3. C. K. Kroell, D. C. Schneider, and A. M. Nahum, "Impact Tolerance and Response of the Human Thorax II", Proceedings of the Eighteenth Stapp Car Crash Conference, December, 1974.

4. R. F. Neathery, "Analysis of Chest Impact Response Data and Scaled Performance Recommendations", Proceedings of the Eighteenth Stapp Car Crash Conference, December, 1974.

5. Gordon R. Plank and Rolf H. Eppinger, "Computed Dynamic Response of the Human Thorax From a Finite Element Model", Twelfth International Technical Conference on Experimental Safety Vehicles, June, 1989.

6. J. O. Hallquist and D. J. Benson, "DYNA3D User's Manual", Lawrence Livermore Laboratories, Report UCID-19592, Rev. 2, March, 1986.

7. Gordon R. Plank and Rolf H. Eppinger, "An Improved Finite Element Model of the Human Thorax" Thirteenth International Technical Conference on Experimental Safety Vehicles, November, 1991.

8. S. B. Roberts and P. H. Chen, "Elastostatic Analysis of the Human Thoracic Skeleton", J. of Biomechanics, Vol. 3, pp. 527-545, Pergamon Press, 1970.

9. L. W. Schneider, D. H. Robbins, M. A. Pflug and R. G. Snyder, "Anthropometry of Motor Vehicle Occupants", Vol. 1, Report No. UMTRI-83-53-1, The University of Michigan Transportation Research Institute, Contract No. DTNH22-80-C-07502, December, 1983.

10. D. H. Robbins, "Anthropometry of Motor Vehicle Occupants", Vol. 2, Report No. UMTRI-83-53-2, The University of Michigan Transportation Research Institute, Contract No. DTNH22-80-C-07502, December, 1983.

11. D. R. Cahill and M. J. Orland, Atlas of Human Cross-Sectional Anatomy, Lea & Febiger, 1984.

12. S. H. Sundaram and C. C. Feng, "Finite Element Analysis of the Human Thorax", Journal of Biomechanics, Vol. 10, pp. 505-516, 1977

13. David C. Viano, Biomechanics of Bone and Tissue: A Review of Material Properties and Failure Characteristics", Paper No. 861923, 1986

14. L. Z. Shuck and S. H. Advani, "Rheological Response of Human Brain Tissue in Shear", Transactions of the ASME, Journal of Basic Engineering, ASME Paper No. 72-WA/BHF-2, 1972

15. A. M. Nahum and J. Melvin, The Biomechanics of Trauma, Prentice Hall, 1985.

16. Y. C. Fung. Biomechanics - Mechanical Properties of Living Tissues, Springer-Verlag, New York, 1981, Chapter 12.

17. J. G. Pinto and P. J. Patitucci, "Visco-Elasticity of Passive Cardiac Muscle", Journal of Biomechanical Engineering, Vol. 102, February, 1980.

18. J. T. Wang and Donald J. Nefske, "A New CAL3D Airbag Inflation Model", SAE Paper Number 880654, 1988

19. J. T. Fleck, "Validation of the Crash Victim Simulator," Volumes I through IV, Report No. DOT-HS-806 279, December 1981.